Journal of Inflammation Research

Dovepress
Taylor & Francis Group

Open Access Full Text Article

ORIGINAL RESEARCH

MAP17 is a Novel NASH Progression Biomarker Associated with Macrophage Infiltration, Immunotherapy Response, and Oxidative Stress

Zhiwei Huang[1,*], Jiatong Chen[1,*], Shenglu Liu[1], Xin Xiang[2], Yang Long[3], Peng Tan[1,4], Wenguang Fu[1,4]

[1]Department of General Surgery (Hepatopancreatobiliary Surgery), The Affiliated Hospital, Southwest Medical University, Luzhou, 646000, People's Republic of China; [2]Department of General Surgery, The First People's Hospital of Neijiang, Neijiang, 641000, People's Republic of China; [3]Department of Endocrinology and Metabolism, The Affiliated Hospital, Southwest Medical University, Luzhou, 646000, People's Republic of China; [4]Metabolic Hepatobiliary and Pancreatic Diseases Key Laboratory of Luzhou City, Academician (Expert) Workstation of Sichuan Province, Department of General Surgery (Hepatopancreatobiliary surgery), The Affiliated Hospital, Southwest Medical University, Luzhou, 646000, People's Republic of China

*These authors contributed equally to this work

Correspondence: Peng Tan; Wenguang Fu, Department of General Surgery (Hepatopancreatobiliary Surgery), The Affiliated Hospital, Southwest Medical University, Luzhou, 646000, People's Republic of China, Email tanpeng@swmu.edu.cn; fuwg@swmu.edu.cn

Background: Nonalcoholic steatohepatitis (NASH) has recently garnered increased attention due to immune infiltration. However, the role of membrane-associated protein 17 (MAP17) in NASH remains unclear, which prompted this study to explore its relationship with immune infiltration and its regulatory mechanisms.

Methods: We employed weighted correlation network analysis (WGCNA) to construct a gene co-expression network aimed at identifying key genes associated with NASH progression. Our further analyses included differential expression evaluation, protein-protein interaction (PPI) network analysis, and Venn diagram analysis to discover novel targets. The CIBERSORT algorithm assessed the correlation between MAP17 and immune cell infiltration within the tumor microenvironment (TME), while the TIDE algorithm predicted responses to immunotherapy. Additionally, we conducted gene ontology (GO), Kyoto Encyclopedia of Genes and Genomes (KEGG), and gene set enrichment analysis (GSEA) to elucidate the mechanisms by which MAP17 operates. The expression of MAP17 was validated using liver tissues obtained from NASH patients and mice with diet-induced NASH or CCl4-induced liver fibrosis.

Results: Our findings identified MAP17 as a novel target in the progression of NASH. Correlation analyses demonstrated a positive association between MAP17 and M1 macrophage infiltration, as well as a negative association with M2 infiltration. TIDE results positioned MAP17 as a potential biomarker for predicting responses to immune checkpoint blockade. Mechanistic studies revealed that MAP17 induced oxidative stress, which subsequently activated the p53, PI3K-AKT, and Wnt signaling pathways. Validation analyses confirmed that MAP17 levels significantly increased in liver tissues of mice with diet-induced NASH or CCl4-induced liver fibrosis, as well as in NASH patients.

Conclusion: MAP17 is a novel biomarker linked to macrophage infiltration and immunotherapy responses in NASH patients. The oxidative stress induced by MAP17 activates the p53, PI3K-AKT, and Wnt pathways, all of which contribute to the progression of NASH.

Keywords: NASH, MAP17, macrophage infiltration, immunotherapy response, oxidative stress

Introduction

Nonalcoholic steatohepatitis (NASH) is a severe stage of hepatic steatosis characterized by ballooning, inflammation, and even fibrosis.[1] Its increased incidence and potential progression to cirrhosis and hepatocellular carcinoma (HCC) have imposed a significant burden on global public health.[2,3] Current biomarkers for detecting, classifying, and monitoring different aspects of NASH, such as steatosis, necroinflammation, or fibrosis, have their limitations in terms of accuracy, reproducibility, responsiveness, feasibility, and economic cost.[4] Moreover, the absence of efficient biomarkers for early

Received: 24 September 2024
Accepted: 8 January 2025
Published: 15 January 2025

detection results in asymptomatic NASH-HCC patients being diagnosed at advanced stages, leading to poor prognoses.[5] While substantial progress has been made in recent years in comprehending the pathogenesis of NASH, it remains incompletely understood.[6] Consequently, the exploration of new biomarkers to enhance our understanding of NASH pathogenesis, aid in early diagnosis, predict disease progression, and pinpoint treatment targets holds significant importance.

The pathogenesis of NASH involves multiple factors, including insulin resistance, the accumulation of lipotoxic substances, and oxidative stress, among others.[7] Recently, the role of immune infiltration in the progression of NASH has become increasingly important.[8,9] Hepatic immune cells exhibit diversity in the steady state and continue to evolve during NASH, directly impacting the disease's severity.[10] Inflammatory signals trigger the recruitment of macrophages, neutrophils, B cells, and other immune cells. The complex interplay between these immune cell populations and hepatocytes or hepatic stellate cells further exacerbates liver injury, fibrosis, and potentially HCC.[11–13] For instance, macrophages, as heterogeneous immune cells, serve as the primary source of cytokines and chemokines in NASH.[14] They can be broadly categorized as M1 type and M2 type. Increased hepatocyte apoptosis prompts macrophages to polarize towards M1, leading to the secretion of TNF-α and CCL2, thereby promoting early NASH stages.[15] Subsequently, the substantial release of cytokines aids in advancing inflammation and fibrosis. Conversely, a decrease in M2 macrophages weakens anti-inflammatory responses. Moreover, macrophages are implicated in regulating lipid metabolism and insulin sensitivity in hepatocytes, contributing to the buildup of lipotoxic substances and metabolic burden on the liver.[16] Immunomodulation-based drugs are currently under investigation. For example, peroxisome proliferator-activated receptor (PPAR) agonists exhibit immunomodulatory properties alongside their lipid metabolism modulation, displaying anti-inflammatory effects on macrophages.[17] Additionally, cenicriviroc, a dual antagonist targeting the chemokine receptors CCR2 and CCR5 expressed in monocytes and T cells, has shown promising results in Phase II trials.[18] Nevertheless, these studies have limitations, and the therapeutic challenges posed by immune cell infiltration and the potential progression to HCC necessitate further research. Therefore, a comprehensive exploration of immune infiltration mechanisms and the identification of new immunotherapeutic targets may enhance potential clinical outcomes for NASH and NASH-associated HCC.

Hepatic oxidative stress plays a key role in the development of NASH.[19] Hepatocytes oxidative stress alters macrophage populations, resulting in an imbalance between M1 and M2 polarization, primarily favoring polarization towards the M1 phenotype and reducing anti-inflammatory M2 macrophages.[20] Moreover, oxidative stress triggers the activation of multiple signals and speeds up the progression of NASH, potentially leading to HCC. For instance, reactive oxygen species (ROS) activate p53, and suppressing p53 activity helps alleviate hepatic steatosis by enhancing HMGB1-associated autophagy.[21,22] Notably, p53 plays a crucial role as a central gene in the advancement from NASH to HCC.[23] Additionally, oxidative stress activates the PI3K-AKT pathway, further expediting the shift from steatosis to NASH and the progression from NASH to HCC.[24] In summary, inhibiting oxidative stress has demonstrated benefits in reducing immune cell infiltration and delaying the malignant advancement of NASH.

The membrane-associated protein 17 (MAP17), also known as PDZK1IP1, is a small, non-glycosylated protein that usually localizes to the plasma membrane. MAP17 has a C-terminal PDZ domain that interacts with its ligand PDZK1 to form a variable complex, enabling the transport of different molecules across the plasma membrane.[25,26] Previous studies have shown that MAP17 mediates multiple signaling pathways, especially promoting inflammation and oxidative stress. MAP17 activates Notch inflammatory signaling, leading to an increase in stem cell factors and cancer-initiating-like cells.[27] MAP17 induces the expression of genes such as NFAT2 and IL-6, which directly regulate the differentiation of monocytes into dendritic cells.[28] Additionally, MAP17 is a ROS-dependent oncogene that enhances the malignant behavior of tumor cells by increasing ROS.[29] More notably, some researchers believe that upregulation of MAP17 is a crucial point in cancer and inflammatory diseases.[30] These pieces of evidence are enough to demonstrate the importance of MAP17 in the regulation of inflammation, immunity, and even as a key target for disease progression. These evidences are sufficient to demonstrate the importance of MAP17 in the regulation of inflammation, immunity and even as a key target for disease progression. However, the role of MAP17 in NASH remains unclear. Therefore, it is of paramount importance to investigate the role of MAP17 in NASH from the perspective of immune infiltration, in order to uncover the underlying mechanisms of disease onset and progression and identify novel therapeutic targets.

Materials and Methods

Data Acquisition

The GEO dataset was obtained from the GEO database (http://www.ncbi.nlm.nih.gov/geo). Specifically, the GSE135251 dataset comprised 206 human NASH samples at various stages of pathogenesis and 10 control samples. From the GSE164760 dataset, 6 healthy liver samples, 74 NASH samples, 8 liver cirrhosis samples, 29 non-tumoral adjacent samples, and 53 NASH-HCC samples were extracted. Additionally, data from 143 human NAFLD/NASH patients is available under the accession number GSE162694. The GSE119340 dataset contained three mouse NASH samples and three normal mouse liver tissues.

Weighted Gene Co-Expression Analysis (WGCNA)

The normalized gene expression data was used to perform WGCNA. The co-expression network was constructed utilizing the WGCNA package in R (version 4.3.1). Pearson's correlation coefficient was employed to obtain gene co-expression similarity measures and to construct an adjacency matrix using soft power and topological overlap matrix (TOM). By applying soft thresholds, correlation matrices were transformed to mimic scale-free topologies. TOM was utilized to filter weak connections during network construction. Module identification was based on TOM and average linkage hierarchical clustering. Adhering to the scale-free topology criterion, a soft power β of 6 (scale-free R^2 of 0.9) was selected. Ultimately, the dynamic tree cut algorithm was employed to select branches in the dendrogram. The module eigengene (ME) was defined as the first principal component of a given module, which could be considered a representative of the gene expression profiles within a module. Module Membership (MM), also known as eigengene-based connectivity (kME), was defined as the correlation of each gene expression profile with the module eigengene of a given module.

Gene Ontology (GO) Analysis

Using Metascape software, we conducted a GO enrichment analysis to identify the functional classes. Three primary GO categories were annotated to transcripts: biological process (BP), cellular component (CC), and molecular function (MF). Additionally, we performed Kyoto Encyclopedia of Genes and Genomes (KEGG) pathway enrichment analysis using Metascape to identify crucial pathways.

Protein-Protein Interaction (PPI) Network

The Search Tool for the Retrieval of Interacting Genes (STRING) (http://string-db.org) was capable of converting DEGs into expressed proteins and constructing a PPI network. We obtained a PPI network of common DEGs using STRING and visualized it with Cytoscape (version 3.7.2).

CIBERSORT Algorithm

The CIBERSORT algorithm (http://cibersortx.stanford.edu) was employed to estimate the composition of 22 distinct immune cell types in the GSE135251 and GSE162694 datasets. The Spearman method was utilized to analyze the correlation between MAP17 expression and the abundance of infiltrating immune cells. Heatmaps and scatter plots were created using the ggpubr and ggplot2 packages in R software (version 4.3.1).

TIDE Score

The TIDE score table, which comprised the TIDE score, exclusion of immune rejection, and dysfunction, was retrieved from the TIDE database (http://tide.dfci.harvard.edu/). Subsequently, the Wilcoxon test was conducted on the TIDE scores from various samples within the GSE164760 and GSE135251 datasets. The test results were visualized as bar graphs. Moreover, the correlation between MAP17 expression and TIDE score in the GEO datasets (GSE164760, GSE135251, and GSE162694) was examined through a scatterplot.

Gene Set Enrichment Analysis (GSEA)

Gene Set Enrichment Analysis (GSEA, http://www.gsea-msigdb.org/) was a popular enrichment analysis method based on Gene sets, which had been widely used in bioinformatics and computational biology research. GSEA ranked all genes analyzed by expression arrays according to their differential expression between two categories of samples, specifically, MAP17 high and MAP17 low. Through this process, GSEA calculated a normalized enrichment score (NES) for each gene set. Positive NES values represented enrichment at the top of the list, while negative NES values represented enrichment at the bottom of the list. The pathway map for GSEA enrichment analysis was then drawn using R (version 4.3.1), which provided a graphical representation of the enriched biological pathways.

Human Liver Samples

Human NASH liver specimens were retrieved from patients who underwent hepatectomy at the Affiliated Hospital of Southwest Medical University due to benign conditions such as hepatic hemangioma and intrahepatic bile duct stones. The specimens were independently assessed by two pathologists based on NAFLD activity scores (NAS). Hepatic steatosis caused by hepatitis B virus, alcohol consumption, etc, was excluded. Normal control liver specimens were obtained, featuring the absence of NASH. Prior to surgery, informed consent for tissue collection was obtained from patients. The study was approved by the Ethics Committee of Southwest Medical University (KY2022167) and was conducted in accordance with the 1975 Declaration of Helsinki.

Animal Models and Sample Collection

Wild-type (WT) mice, based on a C57BL/6J background, were obtained from Vital River Laboratory Animal Technology in Beijing, China. The mice were housed in a temperature-controlled and humidity-controlled experimental animal room. After breeding, 6-8-week-old male WT mice were fed either a control diet or a high-fat diet (HFD, TP26300, Trophic) containing 21.2% fat, 49.1% carbohydrate, 19.8% protein, and 0.2% cholesterol for 24 weeks (n=5 per group). HFD-induced NASH fibrosis mouse models were generated by intraperitoneal injection of 20% CCL4 at a dose of 1 mL/kg once a week, in conjunction with an HFD diet, for 12 weeks (n = 5 per group). For the purpose of inducing hepatic fibrosis via CCL4 administration, mice were intraperitoneally injected with 20% CCL4 at a dose of 2.5 mL/kg twice a week for a duration of 8 weeks (n = 5 per group). The control group received the same dose of vehicle, olive oil. At the conclusion of the feeding period, serum and tissues were collected for subsequent experiments. All animal experiments were performed in accordance with the guidelines set forth by the Animal Experimentation Ethics Committee of Southwest Medical University.

H&E Staining

The fresh liver tissues fixed in 4% paraformaldehyde and embedded in paraffin were utilized for further staining. For H&E staining, sections of 4 μm thickness were cut and sequentially stained with hematoxylin and eosin according to the manufacturer's instructions (G1120, Solarbio). Two pathologists evaluated the H&E-stained liver sections individually based on NAS scores, which were determined by the degree of steatosis, inflammation, and hepatocyte ballooning.

Oil Red O Staining

Fresh liver tissue was frozen and then sliced. The sections were rewarmed and dried before being stained. Afterwards, the sections were fixed in 10% formalin for 10 minutes and washed with water. Next, they were soaked in 60% ethanol for 30 seconds after drying, and then immersed in Oil Red O staining solution for 10 minutes. Subsequently, the sections were rinsed with distilled water and stained with hematoxylin. After sealing with glycerin gelatin, the sections were observed under a microscope.

Sirius Red Staining and Masson's Trichrome Staining

For Sirius red staining, paraffin sections were dewaxed and hydrated, followed by staining in Sirius red. Next, sections were dehydrated using anhydrous ethanol and then cleaned in xylene before being sealed with neutral resin. The steps of dewaxing and hydration were applied to Masson's trichrome staining initially. Subsequently, sections were immersed in a solution of

potassium dichromate at 65°C for 30 minutes and then rinsed with distilled water. The subsequent stains were performed sequentially using hematoxylin, ponceau, phosphomolybdic acid, and aniline blue. Finally, sections were differentiated using glacial acetic acid and then dehydrated using anhydrous ethanol before being sealed with neutral resin.

Immunohistochemistry

Paraffin sections were heated in citrate buffer for antigen retrieval. Three percent hydrogen peroxide solution was used to eliminate endogenous peroxidase, and the sections were then blocked with 2% goat serum. The sections were placed flat in a wet box and incubated overnight at 4°C with the anti-MAP17 antibody (ab156014, Abcam, 1:100). The next day, the sections were incubated for 1 hour with a horseradish peroxidase-linked secondary antibody against rabbit at a dilution of 1:5000. Subsequently, DAB horseradish peroxidase color development was performed according to the manufacturer's protocols. Finally, the nucleus was stained with hematoxylin and visualized under the microscope (BX53, Olympus, Tokyo, Japan).

Western Blot

Proteins were extracted from tissues using RIPA lysis buffer (P0013B, Beyotime). Then, equal amounts of protein were separated by 10% SDS-PAGE and transferred to PVDF membrane later. The PVDF membranes were blocked with TBST containing 5% nonfat milk for 1 h, and washed using TBST three times. Incubation with primary antibodies were performed overnight at 4°C with anti-MAP17 (ab156014, Abcam), anti-P53 (10442-1-AP, Proteintech), anti-p-PI3K (YP0224, Immunoway), anti-PI3K (YM3503, Immunoway), anti-p-AKT (66444-1-Ig, Proteintech), anti-AKT (10176-2-AP, Proteintech) and anti-GAPDH (60004-1-Ig, Proteintech) Afterward, the membranes were incubated with secondary antibodies for 1 h at room temperature. Finally, they were detected by the enhanced chemiluminescence (ECL) detection system.

Statistical Analysis

R software (version 4.3.1) was used for the statistical analysis in this study. The results were presented as means ± standard errors of the mean. Student's *t*-test was employed to compare two groups, while one-way analysis of variance was utilized to compare the means of three or more groups. The Spearman correlation coefficient was used to evaluate correlation. A p-value less than the significance level of 0.05 was considered statistically significant in the evaluation of the findings.

Results

Key Gene Relevant to NASH Progression Was Identified

To identify key genes associated with the progression of NASH, we employed WGCNA in combination with other bioinformatics methods to analyze the GSE135251 dataset. Initially, the input dataset for WGCNA construction consisted of 18296 gene expression profiles and the pathological status of 154 NASH samples (Figure S1A). After quality assessment, a power of $\beta = 6$ (scale-free $R^2 = 0.9$) was selected to construct a scale-free network, resulting in 9 co-expression modules (Figure S1B). We then performed a network heatmap and found that all gene expressions within each module were independent (Figure 1A). Subsequently, we assessed the relevance of eigengenes of each module and NASH fibrosis progression via Module-Trait Relationships (MTRs). The results showed that the eigengenes of the yellow module presented the highest positive correlation with NASH fibrosis progression (Figures 1B and S1C). Furthermore, we performed DEGs analysis using the GSE164760 dataset to identify key genes involved in the progression from NASH to HCC. The volcanogram results indicated that, compared to NASH, 629 genes were significantly upregulated and 915 genes were significantly downregulated in NASH-HCC (Figure 1C). We then constructed a heatmap showing the 629 upregulated DEGs in the GSE164760 dataset (Figure 1D). The Venn diagram revealed the intersection between yellow module genes and upregulated DEGs, identifying 110 key genes associated with NASH progression (Figure 1E). Subsequently, we conducted PPI analysis on the 110 hub genes and constructed a PPI network (Figure 1F). Finally, we performed GO analysis on the 110 key genes associated with NASH progression. In the BP category, extracellular

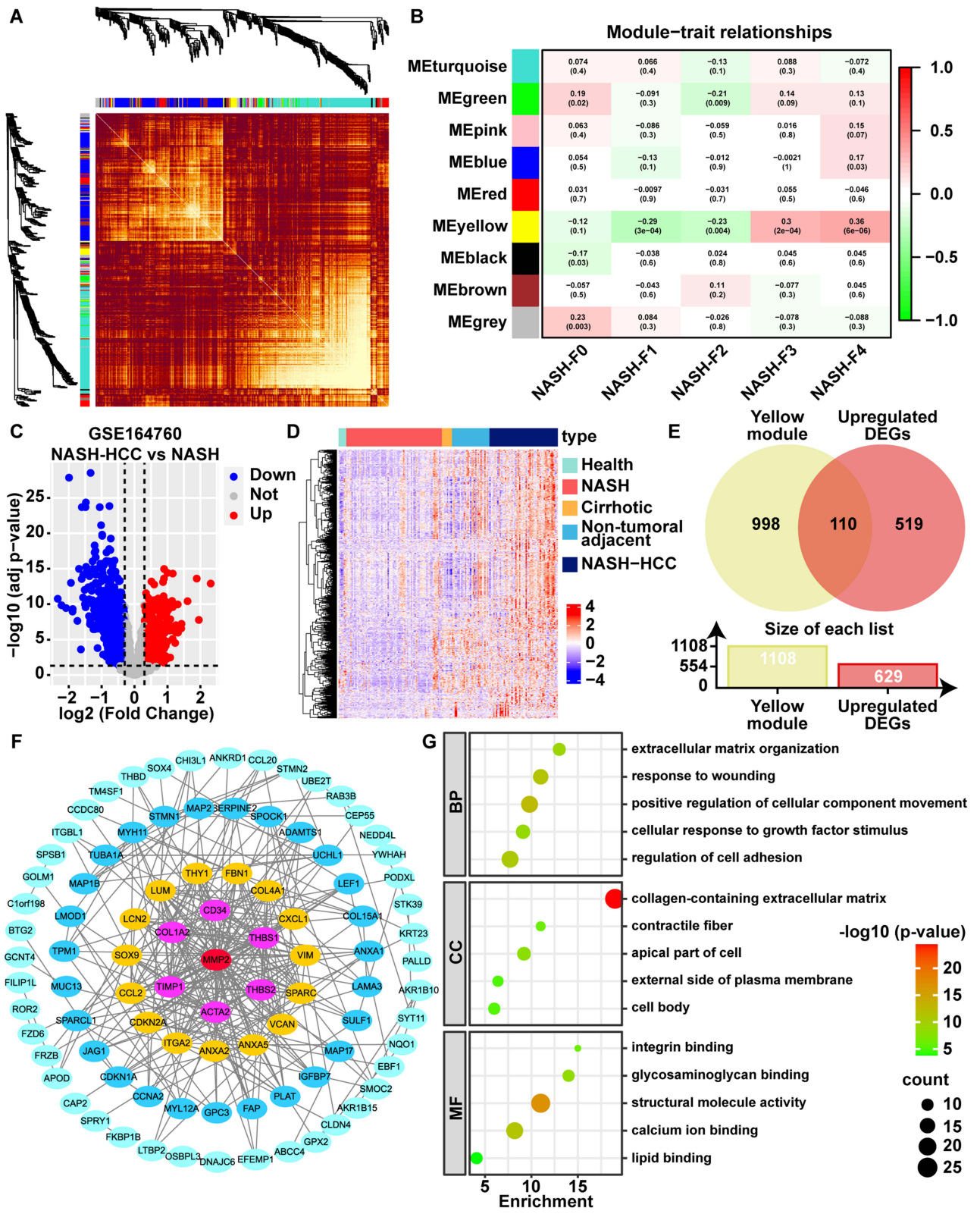

Figure 1 Identification of key genes associated with NASH progression. (**A**) Heatmap of interaction analysis of co-expressing genes. Different colors represent different degrees of overlap. (**B**) Heatmap of the correlation between module eigengenes and fibrosis grade of NASH. Numbers denote correlation (numbers in brackets are P-values). (**C**) The volcano map of GSE164760 revealing DEGs between NASH-HCC and NASH group. (**D**) Heatmap of the 629 upregulated DEGs in the GSE164760 dataset. (**E**) Venn diagram showing overlapping between yellow module genes and upregulated DEGs. (**F**) PPI network for 110 key genes. (**G**) BP, CC, and MF analysis of 110 key genes.

 https://doi.org/10.2147/JIR.S497737

matrix organization was the most enriched. In the CC category, collagen-containing extracellular matrix showed the highest enrichment. Integrin binding exhibited the highest enrichment in the MF category (Figure 1G).

MAP17 as a Novel Target in NASH Progression

To identify key genes involved in NASH progression, we analyzed DEGs in human and mouse NASH livers compared to healthy controls using two public datasets (GSE135251 and GSE119340). Our results revealed that 2,119 DEGs were present in human NASH livers compared to healthy controls, with 1,676 genes upregulated and 443 genes downregulated. Similarly, 2,989 DEGs were identified in mouse NASH livers, comprising 2,448 upregulated and 541 downregulated genes (Figure 2A). To find co-expressed genes between upregulated DEGs and NASH progression key genes, we applied the Venn diagram analysis (Figure 2B). Seven overlapping genes (AKR1B10, ANKRD1, ANXA2, CDKN1A, LTBP2, MAP17, and SPSB1) were identified as candidate hub genes, which might play a vital role in the formation and progression of NASH. Using the GEPIA2 database, we further analyzed the expression of these 7 core genes in liver hepatocellular carcinoma (LIHC). The results showed that the expression levels of only AKR1B10, ANXA2, and MAP17 were significantly higher in LIHC than in normal tissues (Figure 2C). Furthermore, we analyzed the expression of the above three genes in the NASH fibrosis dataset (GSE135251) and the NASH-HCC dataset (GSE164760). The expression levels of AKR1B10, ANXA2, and MAP17 were found to increase with disease stage (F0-F4) in NASH samples (all $p < 0.05$) (Figure 2D). At the same time, we discovered that AKR1B10, ANXA2, and MAP17 were linked to the progression from NASH to cirrhosis to HCC, with the highest expression observed in patients with NASH-associated HCC (all $p < 0.05$) (Figure 2E). AKR1B10 and ANXA2 have been demonstrated to play an important role in the progression of NASH and fibrosis. However, the function of MAP17 in NASH progression remains unknown. This suggests that MAP17 may be a novel target for NASH progression research.

High Expression of MAP17 Was Associated with High M1 Macrophages Infiltration

Immune cell infiltration was shown to play a crucial role in the development and progression of NASH in previous studies. To better understand the underlying mechanism of MAP17, we explored the interaction between MAP17 and immune cell infiltration. We used the CIBERSORT algorithm to evaluate immune infiltration in the GSE135251 dataset and found that M2 macrophages and CD4+ memory resting T cells had higher abundance compared to other immune cells (all $p < 0.05$) (Figure 3A). We also observed significant differences in the infiltration abundance of 8 immune cells, including M2 macrophages, naive B cells, M1 macrophages, NK cells resting, Monocytes, Mast cells resting, Plasma cells, and Regulatory T cells, among the normal, NASH, and NAFL groups (all $p < 0.05$) (Figure 3A). Furthermore, we analyzed the correlation between MAP17 expression and the infiltration abundance of these immune cells using two NASH patient datasets (GSE135251 and GSE162694). Our results showed that the correlation between MAP17 and M1/M2 macrophage infiltration was the only one consistent across both databases (Figure 3B). As depicted in Figure 3C, MAP17 expression was significantly positively correlated with M1 macrophage infiltration and negatively correlated with M2 macrophage infiltration. Finally, our analysis of NASH fibrosis grades revealed that the infiltration level of M1 macrophages gradually increased as the degree of NASH fibrosis increased (Figure 3D), which was consistent with the expression trend of MAP17 across NASH fibrosis grades.

MAP17 Was Significantly Negatively Correlated with Immunotherapy Response

Previous studies have shown limited therapeutic efficacy of immunotherapy for NASH-HCC. To investigate the reasons behind this phenomenon, we analyzed the expression of eight immune checkpoint genes in NASH, cirrhosis, and NASH-HCC (Figure 4A). The results showed that in addition to LAG3 and TIGIT, there were significant differences between groups in the other six immune checkpoint genes (CD274, CTLA4, HAVCR2, PDCD1, PDCD1LG2, and SIGLEC15). Furthermore, we calculated the TIDE score for patients with NASH, cirrhosis, and NASH-HCC to assess their immune evasion ability. The results indicated that the NASH-HCC group had the highest TIDE score, suggesting that immunotherapy was least effective in this group (Figure 4B). Similar results were observed in patients with NASH at stage 4 fibrosis (Figure 4C). To explore the relationship between MAP17 and immunotherapy, we analyzed the correlation between MAP17 expression and eight immune checkpoint genes in NASH patients (Figure 4D). The results showed a significant positive correlation between MAP17 and five immune checkpoint genes (CD274, CTLA4, PDCD1, PDCD1LG2, and SIGLEC15). Additionally, the correlation analysis between MAP17 and TIDE score revealed that higher MAP17 expression was associated with a higher TIDE

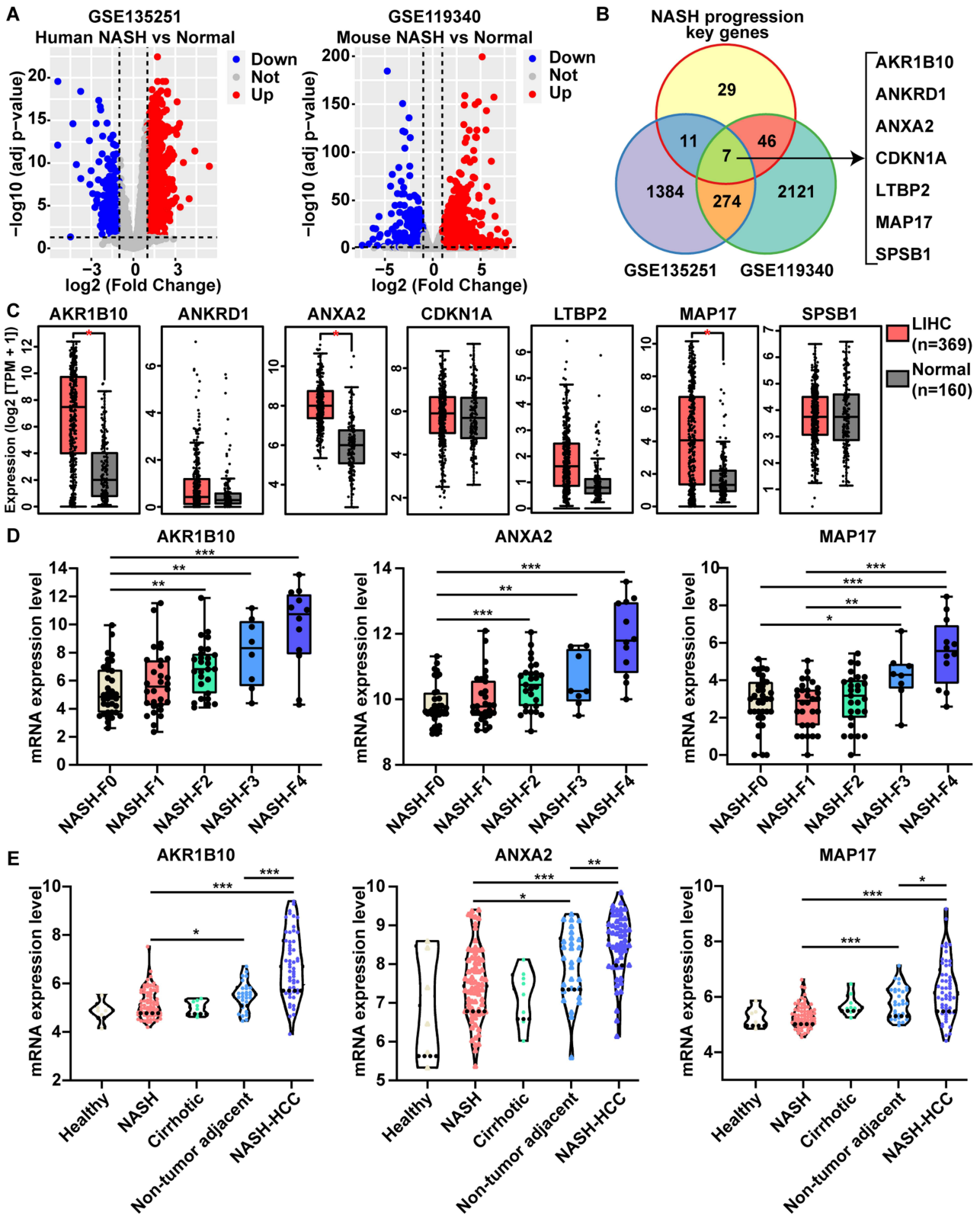

Figure 2 Comprehensive bioinformatics analysis identified MAP17 as a novel target for NASH development. (**A**) Volcano plot displaying log2 (fold change) and −log (adjusted p-value) for the comparison between NASH and control. Red dots represent DEGs with an adjusted p-value ≤ 0.05 and log2 (fold change) ≥ 1.0. Blue dots represent DEGs with an adjusted p-value ≤ 0.05 and log2 (fold change) ≤ −1.0. (**B**) Venn diagram to screen out overlapped hub genes. (**C**) The expression of AKR1B10, ANKRD1, ANXA2, CDKN1A, LTBP2, MAP17, and SPSB1 in human LIHC was analyzed using the GEPIA2 database. (**D**) Using the GSE135251 dataset, we examined the gene expression levels of NASH patients with different stages of fibrosis. (**E**) The differential expression of AKR1B10, ANXA2, and MAP17 among NASH, cirrhosis, and NASH-HCC in the GSE164760 dataset. * $p < 0.05$, ** $p < 0.01$, *and* *** $p < 0.001$.

 https://doi.org/10.2147/JIR.S497737

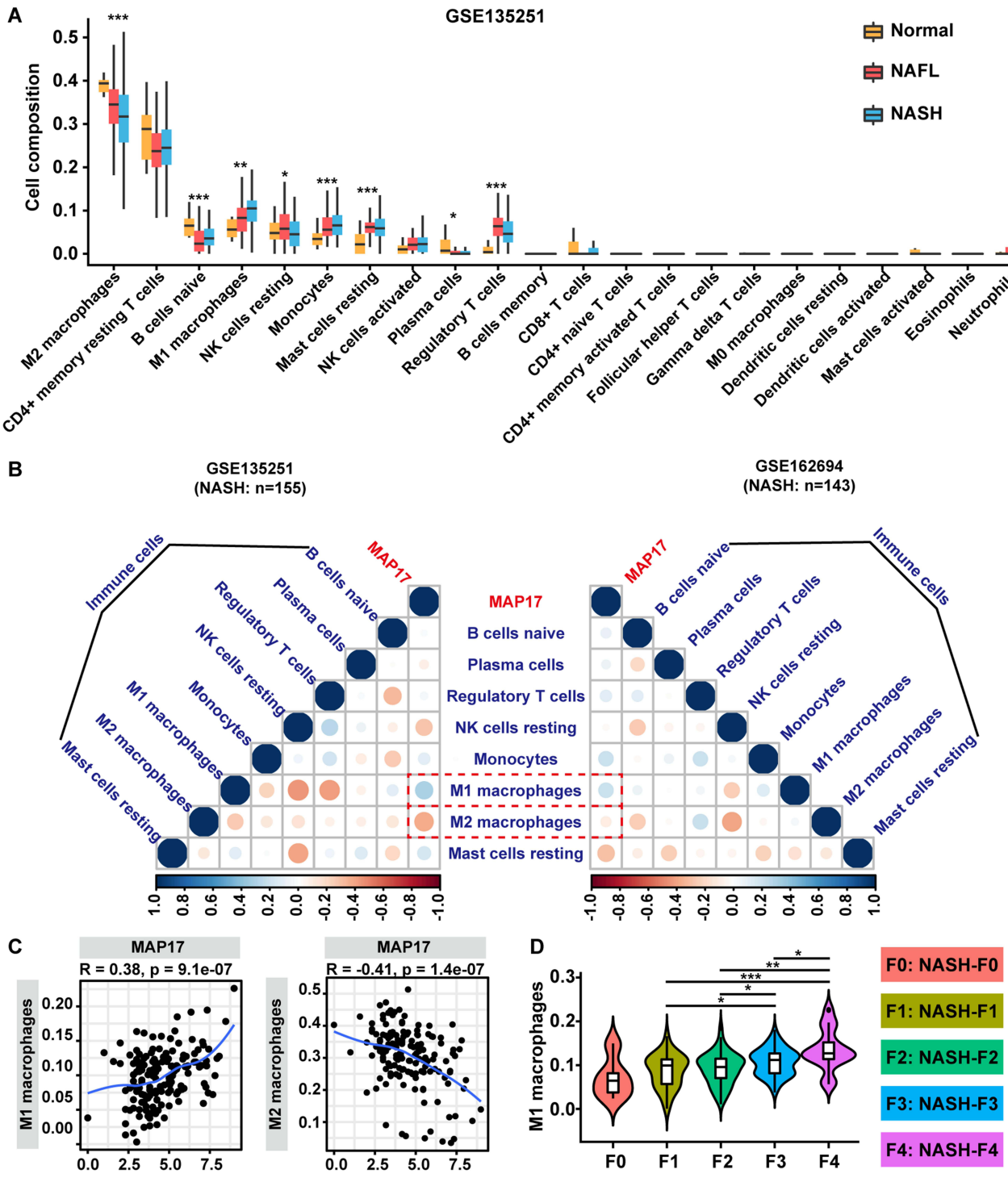

Figure 3 Correlation analysis between MAP17 and immune cell infiltration in NASH. (**A**) The GSE135251 dataset was utilized to evaluate immunity infiltration via the CIBERSORT algorithm. The bar chart showing the infiltration abundance of 22 immune cells in healthy control, NAFL, and NASH groups. (**B**) The correlation heatmap showed the relationship between MAP17 gene expression and 8 immune cells (M2 macrophages, naive B cells, M1 macrophages, resting NK cells, monocytes, resting mast cells, plasma cells, and regulatory T cells) across two NASH patient datasets (GSE135251 and GSE162694). (**C**) Scatter plot showing the correlation between MAP17 expression and M1/M2 macrophage infiltration in GSE135251 dataset. (**D**) The violin plot depicted the M1 macrophage infiltration level of different NASH fibrosis grades in GSE135251 dataset. * $p < 0.05$, ** $p < 0.01$, *and* *** $p < 0.001$.

score, indicating a poorer response to immunotherapy (Figure 4E). These findings suggested that MAP17 had a significant negative correlation with immunotherapy response, highlighting its potential as a reliable marker for predicting immunotherapy efficacy.

https://doi.org/10.2147/JIR.S497737

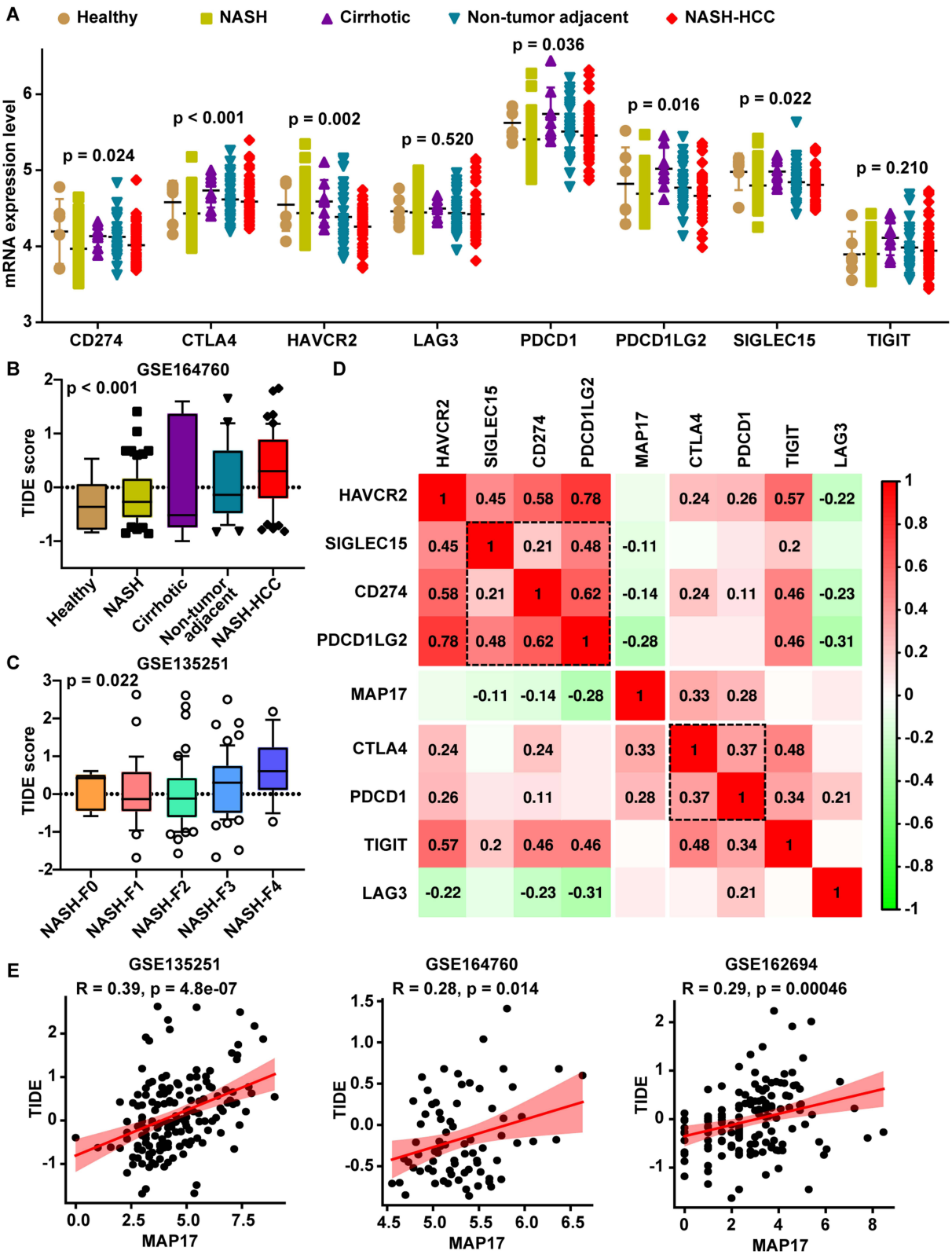

Figure 4 MAP17 expression and immunotherapy response. (**A**) The expression differences of eight immune checkpoint genes among different groups in the GSE164760 dataset. (**B**) Difference analysis of TIDE score of different subtypes in GSE164760 dataset. (**C**) The histogram represented the TIDE score in patients with NASH-mediated liver fibrosis (F0-F4). (**D**) The heatmap showed the correlation between MAP17 and eight immune checkpoint genes in NASH patients from the GSE135251 dataset. (**E**) Correlation scatter plots showed the relationship between MAP17 expression and TIDE score in three datasets (GSE135251, GSE164760, and GSE162694).

https://doi.org/10.2147/JIR.S497737

High MAP17 Expression was Associated with the Activation of the Oxidative Stress Pathway

To investigate the molecular mechanism by which MAP17 affects NASH, we performed KEGG and GSEA analyses previously. Firstly, based on the median MAP17 gene expression level, we divided the GSE162694 cohort into a high expression NASH group and a low expression NASH group. Subsequently, differential expression analysis was conducted between the two groups. Finally, we performed KEGG functional enrichment analysis based on the differentially expressed genes in low and high MAP17 expression in NASH. Figure 5A depicted the network diagram of the top 10 KEGG pathways identified. Concurrently, GSEA revealed that the p53 signaling pathway, PI3K-AKT signaling pathway, and Wnt signaling pathway were enriched in the high MAP17 expression group (Figure 5B). The GSEA verification results in the GSE135251 dataset were consistent with our previous findings (Figure 5C). These highly conserved pathways have been shown to be closely related to oxidative stress in previous studies. Therefore, we further evaluated the relationship between MAP17 and oxidative stress in NASH. Figure 5D displayed the network chart of GO enrichment in biological processes related to the MAP17-mediated oxidative stress response identified. The GSEA analysis further suggested that overexpressed MAP17 may be associated with excessive oxidative stress in NASH (Figure 5E). Consistently, similar results were also observed in the TCGA HCC cohort (Figure 5F). Our findings suggested that MAP17 played an important pathological role in NASH by mediating oxidative stress.

MAP17 is Upregulated in NASH Patients and Mouse Models of NASH

To investigate the expression of MAP17 in the liver tissue of NASH patients and mouse models of NASH, we collected human specimens and established mouse models of NASH by feeding them a HFD diet for 24 weeks. Histological examination of steatosis was confirmed by H&E and Oil Red O staining (Figures 6A and 7A). However, fibrosis is uncommon in clinical NASH patients and some degree of fibrosis occurred in HFD diet-fed mice, but it remained relatively mild according to Masson and Sirius red staining. (Figures 6B and 7B). Our results showed that MAP17 expression was significantly elevated in NASH patients and mouse liver tissues compared to normal tissues, as revealed by immunohistochemistry and Western blot (Figures 6C, 7C, 8A and B). In addition, the infiltration of M1 macrophages and M2 macrophages was evaluated by immunohistochemistry. We observed that CD86, which labels M1 macrophages, was significantly increased in the livers of NASH patients and mouse models, whereas CD206, which labels M2 macrophages, was reduced (Figures 6C and 7C), which further confirms the pro-inflammatory role of M1 macrophages in NASH. Meanwhile, we found that P53 expression was upregulated, and phosphorylation of PI3K and AKT increased (Figure 8A and B), which is consistent with previous studies and suggesting a promotional role of P53 and PI3K-AKT on NASH progression.

MAP17 is Upregulated in CCL4-Induced Fibrosis and HFD-Induced NASH Fibrosis

To investigate the expression of MAP17, we generated two types of hepatic fibrosis mouse models. Histological examination revealed distinct patterns of fibrosis in the liver tissues, as illustrated in Figure 9A and B. Masson and Sirius red staining further confirmed the successful establishment of the fibrosis model, showing significant deposition of collagen (Figure 9A and B). We then performed immunohistochemistry staining on the liver tissues and found that the results were consistent with our previous observations (Figure 9A and B). Notably, our data showed that MAP17 not only exhibited elevated expression in NASH but also displayed high levels of expression in the later stages of liver disease.

Discussion

Nonalcoholic fatty liver disease (NAFLD) was categorized into nonalcoholic simple fatty liver, nonalcoholic steatohepatitis (NASH), and NASH-associated liver fibrosis based on pathological stages. This disease represented a significant public health concern worldwide, with approximately 25% of the global population estimated to be affected, with rates in Asian countries reaching as high as 42%.[31] Research has shown that NASH is more likely to progress to liver fibrosis compared to simple steatosis, yet there were no effective methods available to prevent or treat the disease.[32] Therefore, discovering new targets for NASH therapy was considered crucial. In this study, we identified MAP17, a membrane

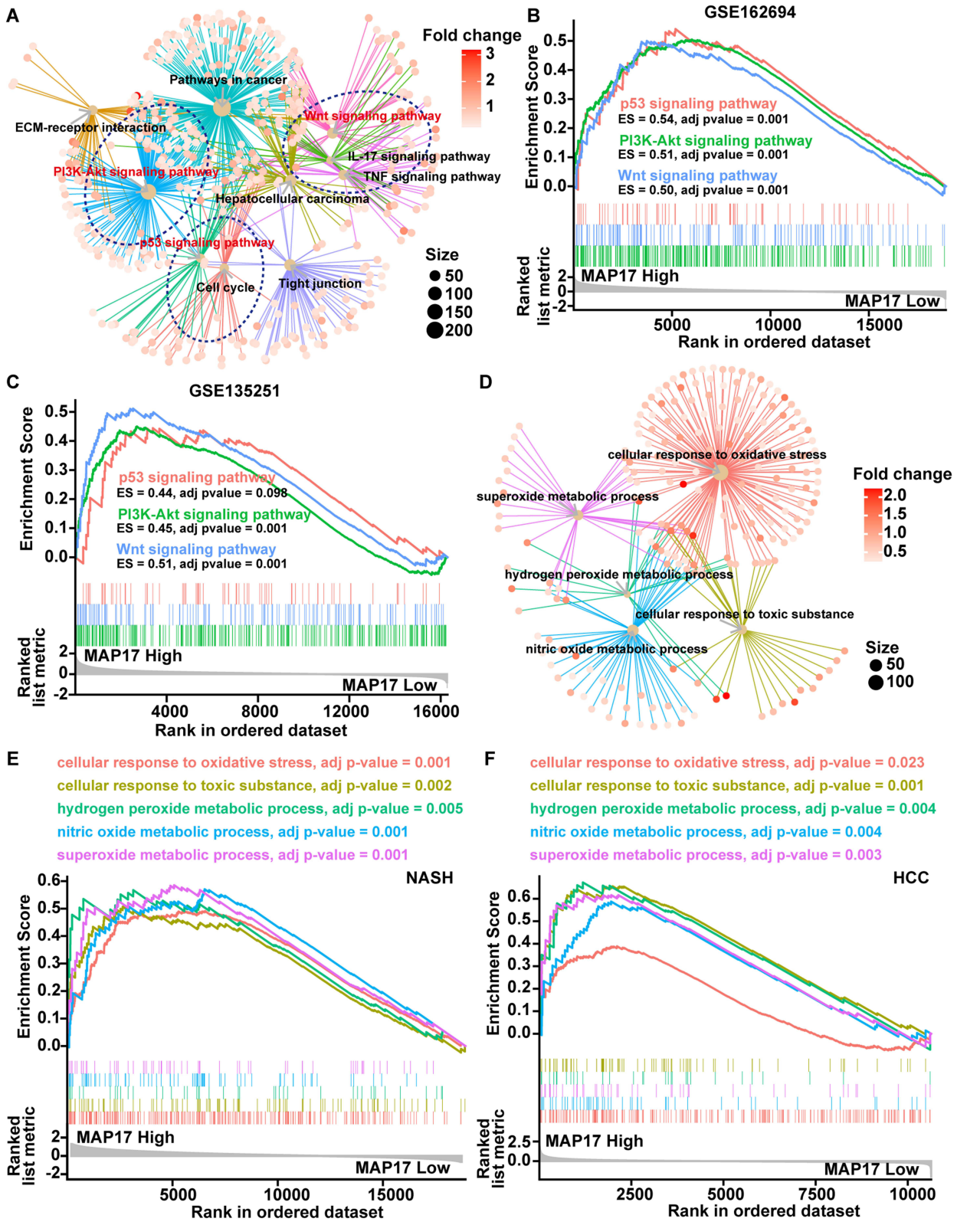

Figure 5 MAP17 expression was positively associated with oxidative stress pathway. (**A**) The KEGG network diagram displayed the top 10 pathways. (**B**) GSEA results showed the p53 signaling pathway, PI3K-AKT signaling pathway, and Wnt signaling pathway, which were differentially enriched in the MAP17-high expression phenotype of the GSE162694 dataset. (**C**) The GSEA analysis for KEGG pathway in the GSE135251 dataset. (**D**) The GO biological processes network diagram displayed the MAP17-mediated oxidative stress response. (**E**) GSEA results showed five oxidative stress-related genes signature, which were differentially enriched in the MAP17-high expression phenotype of the GSE162694 dataset. (**F**) GSEA was applied to determine the MAP17-mediated oxidative stress response in HCC from the TCGA dataset.

https://doi.org/10.2147/JIR.S497737

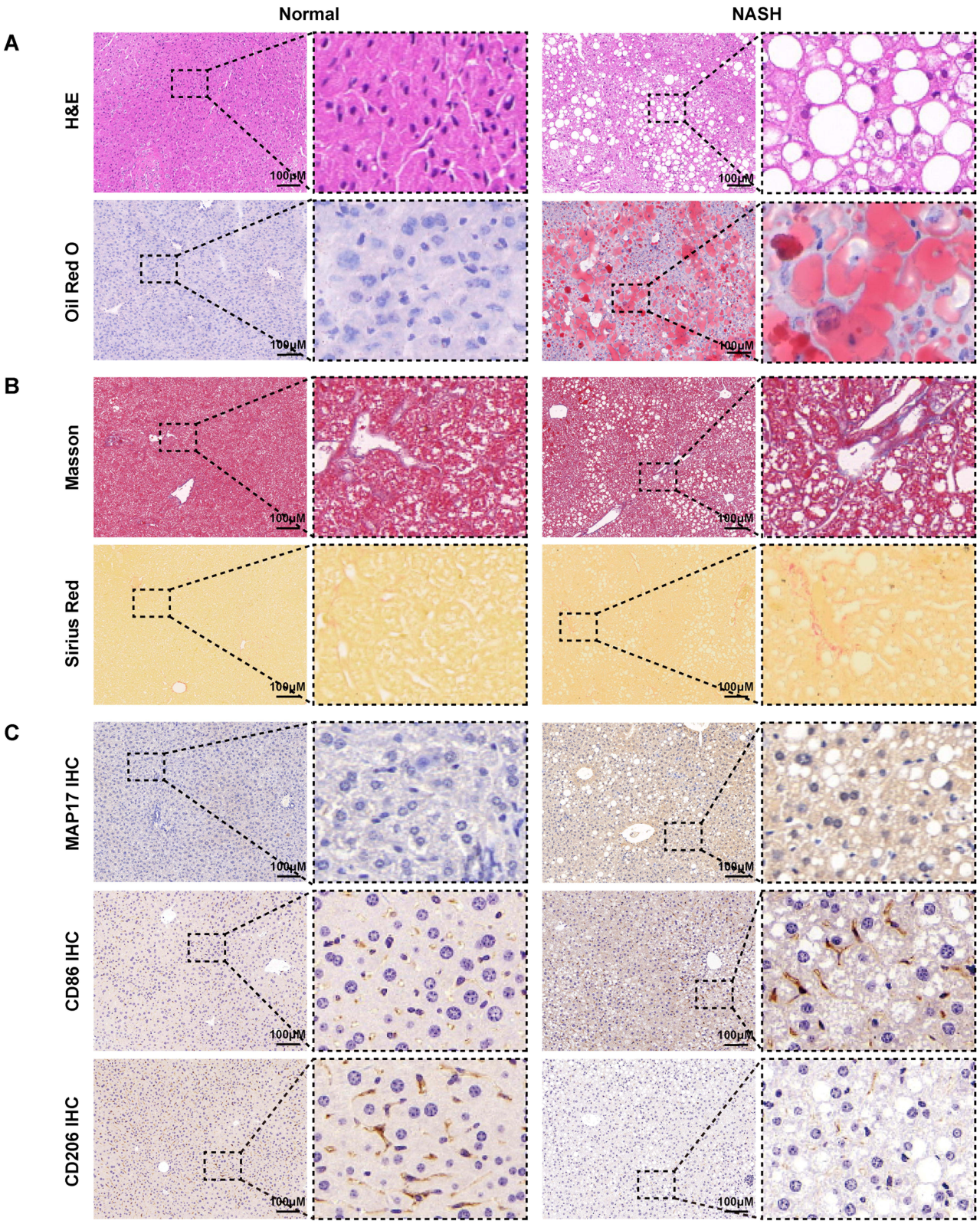

Figure 6 MAP17 is upregulated in NASH patients. (**A**) The representative H&E and Oil Red O staining in liver tissues of NASH patients. (**B**) The representative Masson and Sirius red staining in liver tissues of NASH patients. (**C**) The representative immunohistochemistry of MAP17, CD86 and CD206 in liver tissues of NASH patients. The microscope has a magnification of 100× and the image on the right is a magnification of the image on the left.

https://doi.org/10.2147/JIR.S497737

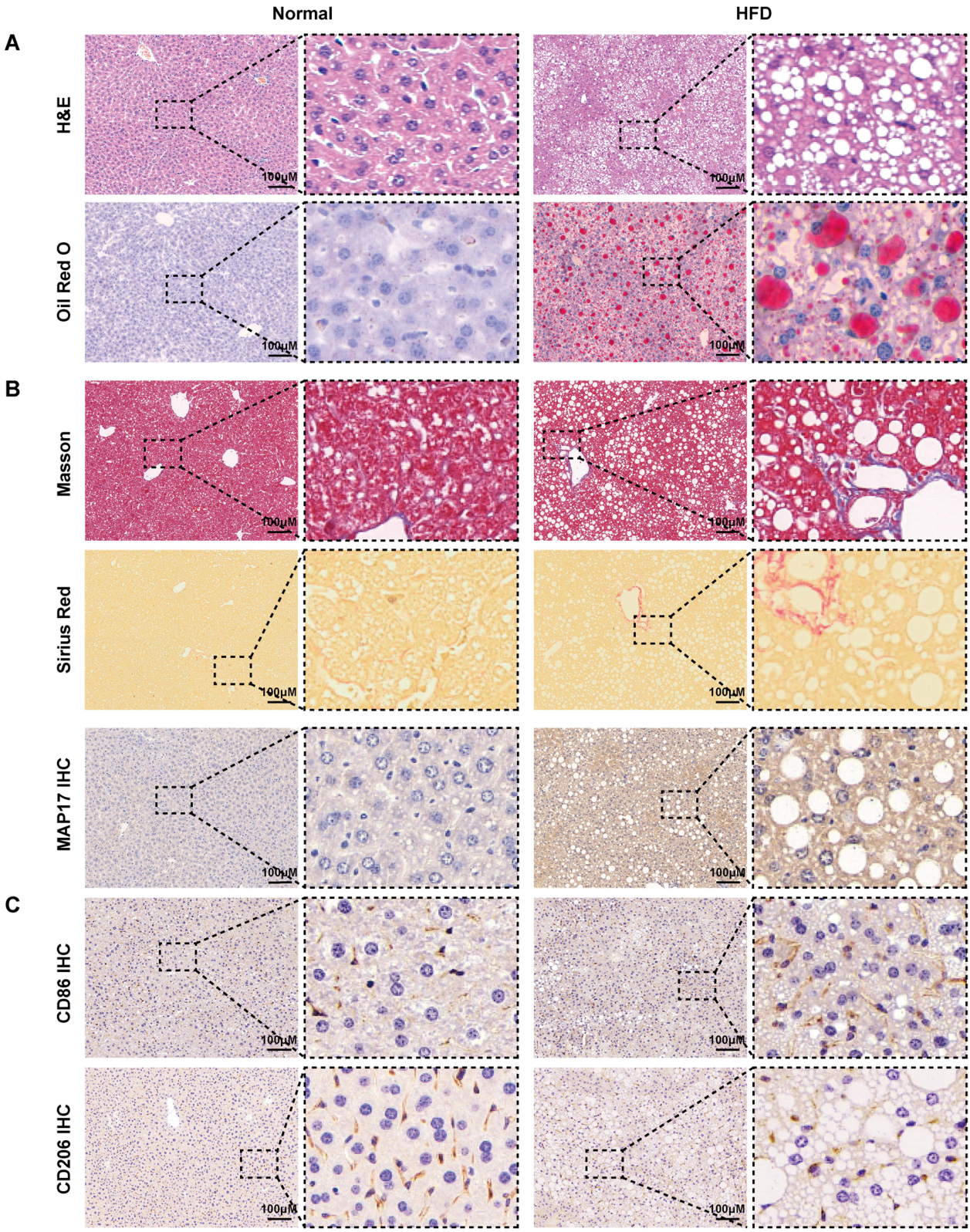

Figure 7 MAP17 is upregulated in mouse models of NASH. (**A**) The representative H&E and Oil Red O staining in liver tissues of mouse models. (**B**) The representative Masson and Sirius red staining in liver tissues of mouse models. (**C**) The representative immunohistochemistry of MAP17, CD86 and CD206 in liver tissues of mouse models. The microscope has a magnification of 100× and the image on the right is a magnification of the image on the left.

https://doi.org/10.2147/JIR.S497737

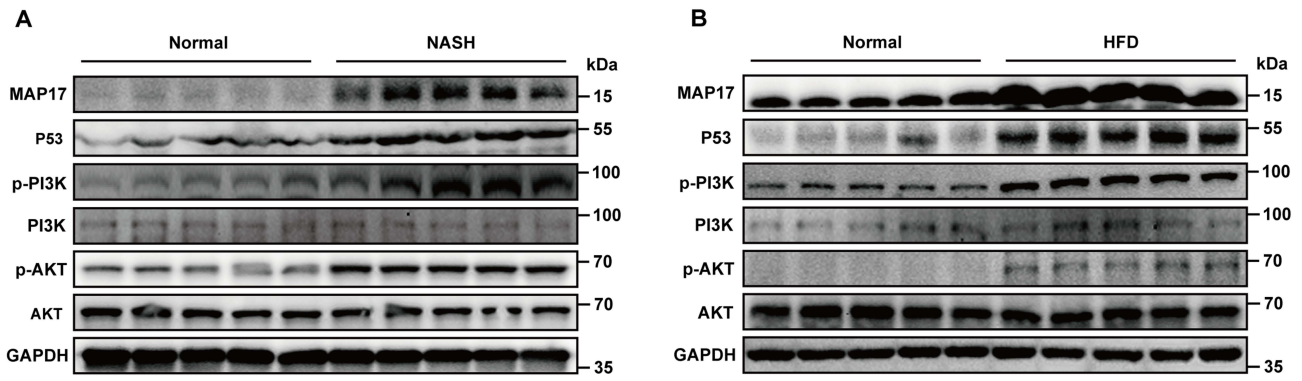

Figure 8 P53 and PI3K-AKT signaling pathway are activated in NASH patients and mouse models of NASH. (**A**) The detection of P53 and PI3K-AKT signaling pathways in liver tissues of NASH patients by Western blot. (**B**) The detection of P53 and PI3K-AKT signaling pathways in liver tissues of mouse models by Western blot.

protein with functions including regulating immunity and inflammation, as a novel target for NASH through comprehensive bioinformatics analysis. MAP17 was found to be highly expressed in liver tissue of NASH patients and mouse models. Further investigation revealed that it served as a novel biomarker for the progression of NASH to fibrosis and even NASH-HCC. Moreover, MAP17 was associated with macrophage infiltration and immunotherapy response, which may be mediated by MAP17-induced oxidative stress.

Macrophage infiltration was a crucial component of NASH immune inflammation, playing a key role in the development of the disease.[33] Two primary sources of liver macrophages have been identified: the resident hepatic macrophages known as Kupffer cells (KCs), which were long established in the liver, and the monocyte-derived macrophages (MoMFs) that were recruited peripherally in response to liver injury.[34,35] KCs were primarily involved in maintaining immune tolerance, preventing excessive immune responses during homeostasis.[36] In contrast, KCs and MoMFs exhibited complementary functions. Upon tissue damage, MoMFs were recruited to the liver,[37] where they were activated and polarized towards a pro-inflammatory M1 phenotype, leading to a gradual accumulation of inflammation.[38] This polarization was accompanied by the secretion of inflammation chemokines such as CXCL10 and TNF-α, which exacerbated hepatic steatosis by inducing lipid accumulation in hepatocytes.[39] Furthermore, MoMFs were found to be widely distributed in fibrotic tissue areas, where they contributed to the progression of fibrosis by inducing the activation of hepatic stellate cells through the secretion of TGF-β1.[40] Given their central role in regulating steatosis, inflammation, and fibrosis in NASH pathogenesis, macrophages emerged as potential target cells in NASH therapy. Considering the regulatory effects of MAP17 on immunity, we explored its relationship with immune cell infiltration in NASH. Our results revealed that MAP17 was significantly positively correlated with M1 macrophage infiltration, while negatively correlated with M2 macrophage infiltration. Notably, we observed a significant positive correlation between the infiltration level of M1 macrophages and MAP17 expression, with a clear and gradual upward trend observed as NASH fibrosis progressed in severity. These findings suggest that MAP17 may be a key target for modulating macrophage infiltration and disease progression in NASH.

In the recent past, the application of immunotherapy in NASH has garnered increasing attention.[41] For instance, PPAR agonists targeting macrophages were developed and evaluated in clinical studies. Although PPARγ and PPARδ were primarily known for regulating lipid metabolism, they displayed antagonistic effects on macrophages, which may have contributed to the potential clinical benefits of NASH.[17] Furthermore, chimeric antigen receptor T cell (CAR-T) therapy targeted hepatic stellate cells and macrophages in NASH for clearance, thereby alleviating fibrosis and injury.[42] Similarly, therapeutic strategies focused on other immune cell subsets were being developed.[18,43] Our study discovered that high MAP17 expression was positively correlated with TIDE score in NASH. This finding may have been a possible mechanism for the insensitivity of NASH to immunotherapy. Targeting MAP17 may have been a potential means to improve immunotherapy for NASH in the future.

As research into NASH and its subsequent HCC evolved, our fundamental understanding of these diseases gradually improved. NASH was increasingly recognized as an inherently aggressive disease.[44,45] Despite advances in disease management aimed at reducing fibrosis progression, NASH ultimately became the leading cause of HCC due to the immune microenvironment, germline mutations, and the microbiome.[46,47] Preclinical studies suggested that immunotherapy efficacy

https://doi.org/10.2147/JIR.S497737

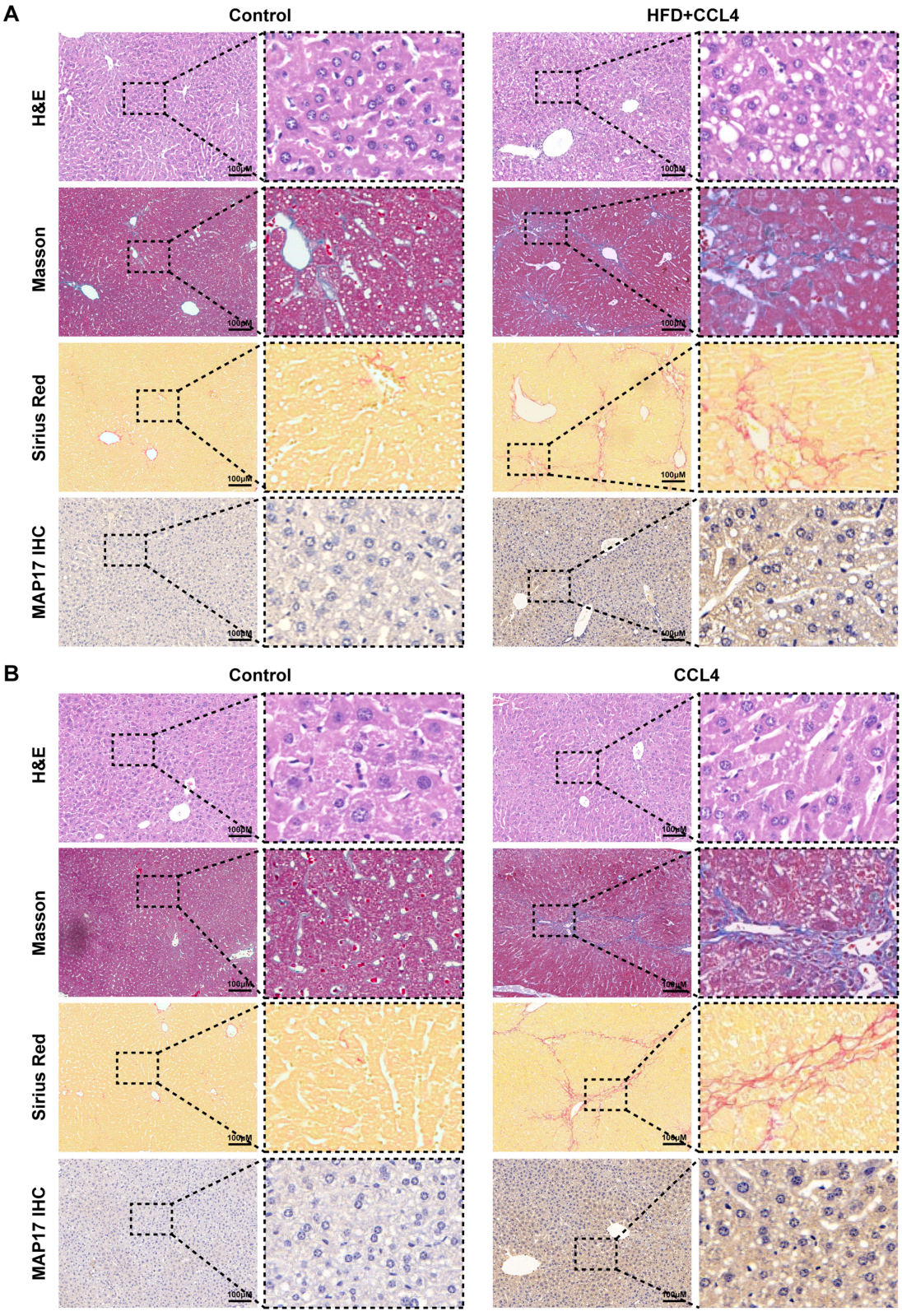

Figure 9 MAP17 is upregulated in CCL4-induced fibrosis and HFD-induced NASH fibrosis. (**A**) The representative H&E, Masson, Sirius red staining and immunohistochemistry of MAP17 in liver tissues of HFD-induced NASH fibrosis. (**B**) The representative H&E, Masson, Sirius red staining and immunohistochemistry of MAP17 in liver tissues of CCL4-induced NASH fibrosis. The microscope has a magnification of 100× and the image on the right is a magnification of the image on the left.

in NASH-HCC may have been reduced compared to virus-induced HCC.[48] Consequently, mechanistic exploration and immune resistance linking NASH progression and immunologic phenotyping analysis were crucial tools for preventing progression to cirrhosis and even HCC, as well as for improving NASH surveillance and ultimately survival in NASH-HCC patients. Our investigation revealed that the TIDE score had been gradually increasing with the progression of NASH, with NASH-HCC reaching its highest point, and this trend was consistent with the expression level of MAP17. Notably, the expression level of MAP17 was found to be positively correlated with the TIDE score, suggesting that MAP17 may have been a possible mechanism of immunosuppression in NASH-HCC. Inhibiting MAP17 may have been an effective means to improve NASH-HCC immune tolerance.

Our study revealed that high MAP17 expression was strongly linked to the activation of oxidative stress in NASH. It is well established that oxidative stress is a crucial component of the multifaceted pathogenesis of NASH.[49] Chronic impairment of lipid metabolism was found to be closely associated with an imbalance of oxidants and antioxidants, which affects metabolism-related organelles, leading to cellular lipotoxicity, lipid peroxidation, and mitochondrial dysfunction. Increased oxidative stress also triggered hepatocellular stress pathways that led to inflammation and fibrosis, thereby promoting the development of NASH.[50] Notably, MAP17 had previously been defined as a ROS-dependent gene,[51,52] and targeting the MAP17/ROS pathway may have been an alternative approach for preventing and treating HCC. Our findings suggested that MAP17-induced oxidative stress was significantly associated with NASH progression, but the specific mechanism by which it regulates NASH progression remained unclear. In-depth mechanistic analysis revealed that MAP17 was closely related to the activation of p53, PI3K-AKT, and Wnt pathways. It was reported that these pathways are involved in regulating pathological processes of NASH such as metabolism, inflammation, and fibrosis.[53–55] Meanwhile, oxidative stress could directly activate the p53, PI3K-AKT, and Wnt/beta-catenin signaling pathways. P53 was recognized as a hub gene for the progression of NASH to HCC, and oxidative stress induced the activation of PI3K-AKT axis, which accelerated the progression of steatosis to NASH and the transition from NASH to HCC.[23,24] Furthermore, previous studies had indicated that oxidative stress resulting from iron overload in NASH activates Wnt/beta-catenin signaling pathways, which may lead to carcinogenesis. Considering the induction effect of MAP17 on oxidative stress, our findings conclusively suggested that MAP17-induced oxidative stress may have promoted the progression of NASH by activating the p53, PI3K-AKT, and Wnt pathways. We believe that an in-depth study of the downstream molecular mechanisms related to MAP17 will be a key research direction. This approach will offer new insights for understanding the pathogenesis of NASH and for selecting diagnostic and therapeutic targets.

Overall, our research provided a potential biomarker for NASH progression, MAP17, which significantly contributes to the early diagnosis, staging, and treatment of NASH-HCC. Targeting MAP17 may be a promising approach to NASH and NASH-HCC immunotherapy.

Data Sharing Statement

GSE135251, GSE164760, GSE162694, and GSE119340 were downloaded from Gene Expression Omnibus (GEO, https://www.ncbi.nlm.nih.gov/geo/).

Funding

This work was supported by the Sichuan Provincial Central Government Leading Local Science and Technology Development Special Project (Grant No. 2023ZYD0073), the National Natural Science Foundation of China (Grant No. 82100679, 82170587), the Sichuan Provincial Natural Science Foundation for Outstanding Youth Foundation (Grant No. 2024NSFJQ0054), the Youth Program of the Natural Science Foundation of Sichuan Province (Grant No. 2023NSFSC1624), the Sichuan Science and Technology Program (Grant No. 2022YFS0617), the Luzhou Science and Technology Plan Project (Grant No. 2023JYJ054, 2023RCM194), and Neijiang First People's Hospital - Southwest Medical University Strategic cooperation project (Grant No. 2021NJXNYD03).

Disclosure

The authors declare that there is no conflicts of interest in this work.

References

1. Adorini L, Trauner M. FXR agonists in NASH treatment. *J Hepatol*. 2023;79(5):1317–1331. doi:10.1016/j.jhep.2023.07.034
2. Hoogerland JA, Staels B, Dombrowicz D. Immune-metabolic interactions in homeostasis and the progression to NASH. *Trends Endocrinol Metab*. 2022;33(10):690–709. doi:10.1016/j.tem.2022.07.001
3. Danpanichkul P, Suparan K, Dutta P, et al. Disparities in metabolic dysfunction-associated steatotic liver disease and cardiometabolic conditions in low and lower middle-income countries: a systematic analysis from the global burden of disease study 2019. *Metabolism*. 2024;158:155958. doi:10.1016/j.metabol.2024.155958
4. Vali Y, Lee J, Boursier J, et al. Biomarkers for staging fibrosis and non-alcoholic steatohepatitis in non-alcoholic fatty liver disease (the LITMUS project): a comparative diagnostic accuracy study. *Lancet Gastroenterol Hepatol*. 2023;8(8):714–725. doi:10.1016/S2468-1253(23)00017-1
5. Tang K, Lin W, Wang D, et al. Potential role of MAP3K14 in hepatocellular carcinoma: a study based on comprehensive bioinformatical analysis and validation. *J Cancer*. 2024;15(9):2731–2745. doi:10.7150/jca.95322
6. Musso G, Saba F, Cassader M, et al. Lipidomics in pathogenesis, progression and treatment of nonalcoholic steatohepatitis (NASH): recent advances. *Prog Lipid Res*. 2023;91:101238. doi:10.1016/j.plipres.2023.101238
7. Yang YY, Xie L, Zhang N-P, et al. Updates on novel pharmacotherapeutics for the treatment of nonalcoholic steatohepatitis. *Acta Pharmacol Sin*. 2022;43(5):1180–1190. doi:10.1038/s41401-022-00860-3
8. Sawada K, Chung H, Softic S, et al. The bidirectional immune crosstalk in metabolic dysfunction-associated steatotic liver disease. *Cell Metab*. 2023;35(11):1852–1871. doi:10.1016/j.cmet.2023.10.009
9. Guo Z, Wu Q, Xie P, et al. Immunomodulation in non-alcoholic fatty liver disease: exploring mechanisms and applications. *Front Immunol*. 2024;15:1336493. doi:10.3389/fimmu.2024.1336493
10. Huby T, Gautier EL. Immune cell-mediated features of non-alcoholic steatohepatitis. *Nat Rev Immunol*. 2022;22(7):429–443. doi:10.1038/s41577-021-00639-3
11. Dudek M, Pfister D, Donakonda S, et al. Auto-aggressive CXCR6(+) CD8 T cells cause liver immune pathology in NASH. *Nature*. 2021;592(7854):444–449. doi:10.1038/s41586-021-03233-8
12. Sierro F, Evrard M, Rizzetto S, et al. A liver capsular network of monocyte-derived macrophages restricts hepatic dissemination of intraperitoneal bacteria by neutrophil recruitment. *Immunity*. 2017;47(2):374–388.e6. doi:10.1016/j.immuni.2017.07.018
13. Koenen RR, von Hundelshausen P, Nesmelova IV, et al. Disrupting functional interactions between platelet chemokines inhibits atherosclerosis in hyperlipidemic mice. *Nat Med*. 2009;15(1):97–103. doi:10.1038/nm.1898
14. Wang H, Mehal W, Nagy LE, et al. Immunological mechanisms and therapeutic targets of fatty liver diseases. *Cell Mol Immunol*. 2021;18(1):73–91. doi:10.1038/s41423-020-00579-3
15. Tosello-Trampont AC, Landes SG, Nguyen V, et al. Kuppfer cells trigger nonalcoholic steatohepatitis development in diet-induced mouse model through tumor necrosis factor-α production. *J Biol Chem*. 2012;287(48):40161–40172. doi:10.1074/jbc.M112.417014
16. Huang W, Metlakunta A, Dedousis N, et al. Depletion of liver Kupffer cells prevents the development of diet-induced hepatic steatosis and insulin resistance. *Diabetes*. 2010;59(2):347–357. doi:10.2337/db09-0016
17. Lefere S, Puengel T, Hundertmark J, et al. Differential effects of selective- and pan-PPAR agonists on experimental steatohepatitis and hepatic macrophages(☆). *J Hepatol*. 2020;73(4):757–770. doi:10.1016/j.jhep.2020.04.025
18. Vuppalanchi R, Noureddin M, Alkhouri N, et al. Therapeutic pipeline in nonalcoholic steatohepatitis. *Nat Rev Gastroenterol Hepatol*. 2021;18(6):373–392. doi:10.1038/s41575-020-00408-y
19. Arroyave-Ospina JC, Wu Z, Geng Y, et al. Role of oxidative stress in the pathogenesis of non-alcoholic fatty liver disease: implications for prevention and therapy. *Antioxidants*. 2021;10(2):174. doi:10.3390/antiox10020174
20. Ni Y, Zhuge F, Nagashimada M, et al. Lycopene prevents the progression of lipotoxicity-induced nonalcoholic steatohepatitis by decreasing oxidative stress in mice. *Free Radic Biol Med*. 2020;152:571–582. doi:10.1016/j.freeradbiomed.2019.11.036
21. Shi T, van Soest DMK, Polderman PE, et al. DNA damage and oxidant stress activate p53 through differential upstream signaling pathways. *Free Radic Biol Med*. 2021;172:298–311. doi:10.1016/j.freeradbiomed.2021.06.013
22. Zhang X, Lin Y, Lin S, et al. Silencing of functional p53 attenuates NAFLD by promoting HMGB1-related autophagy induction. *Hepatol Int*. 2020;14(5):828–841. doi:10.1007/s12072-020-10068-4
23. Liu B, Wang X, Wu N, et al. Hub genes involved in the progression of nonalcoholic fatty liver disease to hepatocellular carcinoma. *Curr Med Chem*. 2024.
24. Grohmann M, Wiede F, Dodd GT, et al. Obesity drives STAT-1-dependent NASH and STAT-3-dependent HCC. *Cell*. 2018;175(5):1289–1306.e20. doi:10.1016/j.cell.2018.09.053
25. Kocher O, Comella N, Gilchrist A, et al. PDZK1, a novel PDZ domain-containing protein up-regulated in carcinomas and mapped to chromosome 1q21, interacts with cMOAT (MRP2), the multidrug resistance-associated protein. *Lab Invest*. 1999;79(9):1161–1170.
26. Pribanic S, Gisler SM, Bacic D, et al. Interactions of MAP17 with the NaPi-IIa/PDZK1 protein complex in renal proximal tubular cells. *Am J Physiol Renal Physiol*. 2003;285(4):F784–91. doi:10.1152/ajprenal.00109.2003
27. Garcia-Heredia JM, Lucena-Cacace A, Verdugo-Sivianes EM, et al. The cargo protein MAP17 (PDZK1IP1) regulates the cancer stem cell pool activating the notch pathway by abducting NUMB. *Clin Cancer Res*. 2017;23(14):3871–3883. doi:10.1158/1078-0432.CCR-16-2358
28. García-Heredia JM, Carnero A. The cargo protein MAP17 (PDZK1IP1) regulates the immune microenvironment. *Oncotarget*. 2017;8(58):98580–98597. doi:10.18632/oncotarget.21651
29. Guijarro MV, Leal JFM, Blanco-Aparicio C, et al. MAP17 enhances the malignant behavior of tumor cells through ROS increase. *Carcinogenesis*. 2007;28(10):2096–2104. doi:10.1093/carcin/bgm124
30. García-Heredia JM, Carnero A. Dr. Jekyll and Mr. Hyde: MAP17's up-regulation, a crosspoint in cancer and inflammatory diseases. *Mol Cancer*. 2018;17(1):80. doi:10.1186/s12943-018-0828-7
31. Younossi ZM, Koenig AB, Abdelatif D, et al. Global epidemiology of nonalcoholic fatty liver disease-meta-analytic assessment of prevalence, incidence, and outcomes. *Hepatology*. 2016;64(1):73–84. doi:10.1002/hep.28431
32. Tilg H, Byrne CD, Targher G. NASH drug treatment development: challenges and lessons. *Lancet Gastroenterol Hepatol*. 2023;8(10):943–954. doi:10.1016/S2468-1253(23)00159-0

33. Yuan Y, Zhang Y, Lu X, et al. Novel insights into macrophage immunometabolism in nonalcoholic steatohepatitis. *Int Immunopharmacol*. 2024;131:111833. doi:10.1016/j.intimp.2024.111833
34. Krenkel O, Tacke F. Liver macrophages in tissue homeostasis and disease. *Nat Rev Immunol*. 2017;17(5):306–321. doi:10.1038/nri.2017.11
35. Tran S, Baba I, Poupel L, et al. Impaired Kupffer cell self-renewal alters the liver response to lipid overload during non-alcoholic steatohepatitis. *Immunity*. 2020;53(3):627–640.e5. doi:10.1016/j.immuni.2020.06.003
36. Wang Y, Heymann F, Peiseler M. Intravital imaging: dynamic insights into liver immunity in health and disease. *Gut*. 2024;73(8):1364–1375. doi:10.1136/gutjnl-2023-331739
37. Wang X, Rao H, Zhao J, et al. STING expression in monocyte-derived macrophages is associated with the progression of liver inflammation and fibrosis in patients with nonalcoholic fatty liver disease. *Lab Invest*. 2020;100(4):542–552. doi:10.1038/s41374-019-0342-6
38. Ning D, Jin J, Fang Y, et al. DEAD-Box Helicase 17 exacerbates non-alcoholic steatohepatitis via transcriptional repression of cyp2c29, inducing hepatic lipid metabolism disorder and eliciting the activation of M1 macrophages. *Clin Transl Med*. 2024;14(2):e1529. doi:10.1002/ctm2.1529
39. Wang Q, Zhou H, Bu Q, et al. Role of XBP1 in regulating the progression of non-alcoholic steatohepatitis. *J Hepatol*. 2022;77(2):312–325. doi:10.1016/j.jhep.2022.02.031
40. Ramachandran P, Dobie R, Wilson-Kanamori JR, et al. Resolving the fibrotic niche of human liver cirrhosis at single-cell level. *Nature*. 2019;575 (7783):512–518. doi:10.1038/s41586-019-1631-3
41. Zhong X, Lv M, Ma M, et al. State of CD8(+) T cells in progression from nonalcoholic steatohepatitis to hepatocellular carcinoma: from pathogenesis to immunotherapy. *Biomed Pharmacother*. 2023;165:115131. doi:10.1016/j.biopha.2023.115131
42. Amor C, Feucht J, Leibold J, et al. Senolytic CAR T cells reverse senescence-associated pathologies. *Nature*. 2020;583(7814):127–132. doi:10.1038/s41586-020-2403-9
43. Newsome PN, Buchholtz K, Cusi K, et al. A placebo-controlled trial of subcutaneous semaglutide in nonalcoholic steatohepatitis. *N Engl J Med*. 2021;384(12):1113–1124. doi:10.1056/NEJMoa2028395
44. Shi YW, Fan JG. Surveillance of the progression and assessment of treatment endpoints for nonalcoholic steatohepatitis. *Clin Mol Hepatol*. 2023;29 (Suppl):S228–s243. doi:10.3350/cmh.2022.0401
45. Rui L, Lin JD. Reprogramming of hepatic metabolism and microenvironment in nonalcoholic steatohepatitis. *Annu Rev Nutr*. 2022;42:91–113. doi:10.1146/annurev-nutr-062220-105200
46. Wang X, Zhang L, Dong B. Molecular mechanisms in MASLD/MASH-related HCC. *Hepatology*. 2024.
47. Miao Y, Li Z, Feng J, et al. The role of CD4(+)T cells in nonalcoholic steatohepatitis and hepatocellular carcinoma. *Int J Mol Sci*. 2024;25 (13):6895. doi:10.3390/ijms25136895
48. Pinter M, Pinato DJ, Ramadori P, et al. NASH and hepatocellular carcinoma: immunology and immunotherapy. *Clin Cancer Res*. 2023;29 (3):513–520. doi:10.1158/1078-0432.CCR-21-1258
49. Clare K, Dillon JF, Brennan PN. Reactive oxygen species and oxidative stress in the pathogenesis of MAFLD. *J Clin Transl Hepatol*. 2022;10 (5):939–946. doi:10.14218/JCTH.2022.00067
50. Myint M, Oppedisano F, De Giorgi V, et al. Inflammatory signaling in NASH driven by hepatocyte mitochondrial dysfunctions. *J Transl Med*. 2023;21(1):757. doi:10.1186/s12967-023-04627-0
51. Carnero A. MAP17, a ROS-dependent oncogene. *Front Oncol*. 2012;2:112. doi:10.3389/fonc.2012.00112
52. Perez M, García-Heredia JM, Felipe-Abrio B, et al. Sarcoma stratification by combined pH2AX and MAP17 (PDZK1IP1) levels for a better outcome on doxorubicin plus olaparib treatment. *Signal Transduct Target Ther*. 2020;5(1):195. doi:10.1038/s41392-020-00246-z
53. Bonnet L, Alexandersson I, Baboota RK, et al. Cellular senescence in hepatocytes contributes to metabolic disturbances in NASH. *Front Endocrinol*. 2022;13:957616. doi:10.3389/fendo.2022.957616
54. Du D, Liu C, Qin M, et al. Metabolic dysregulation and emerging therapeutical targets for hepatocellular carcinoma. *Acta Pharm Sin B*. 2022;12 (2):558–580. doi:10.1016/j.apsb.2021.09.019
55. Shree Harini K, Ezhilarasan D. Wnt/beta-catenin signaling and its modulators in nonalcoholic fatty liver diseases. *Hepatobiliary Pancreat Dis Int*. 2023;22(4):333–345. doi:10.1016/j.hbpd.2022.10.003